11

Particle Swarm Optimization Applied for Locating an Intruder by an Ultra-Wideband Radar Network

Rodrigo M. S. de Oliveira, Carlos L. S. S. Sobrinho, Josivaldo S. Araújo and Rubem G. Farias
Federal University of Pará (UFPA)
Brazil

1. Introduction

As it was shown by the authors in a previous work, the Finite-Difference Time-Domain (FDTD) method is adequate to solve numerically Maxwell's Equations for simulating the propagation of Ultra-Wideband (UWB) pulses in complex environments. These pulses are important in practice in high-resolution radar and GPS systems and in high performance (wideband) wireless communication links, because they are immune to selective frequency fading related to complex environments, such as residences, offices, laboratories among others. In this case, it is necessary to use spread spectrum techniques for transmission, in order to avoid interferences to other wireless systems, such as cell phone networks, GPS, Bluetooth and IEEE802.11. It is worth to mention that by combining these techniques to UWB pulses; it is possible to obtain a signal with power spectrum density under noise threshold, what is a very interesting characteristic for this application.

The proposed simulated environment is a building consisting of several rooms (laboratories) separated by masonry. Internal and external walls are characterized by specific widths and electrical parameters. Wood doors were included in the analysis domain. The analysis region is then limited by U-PML (Uniaxial Perfectly Matched Layers) technique and the system is excited by omni-directional antennas. In order to make the simulations more real, Additive White Gaussian Noise was considered. Aiming at verifying the robustness of the radar network, objects are included in the domain in a semi-random spatial distribution, increasing the contribution of the wave scattering phenomena. Omni-directional antennas were used to register transient electric field in specific points of the scenery, which are adequate for the propose of this work. From those transient responses, it is possible to determine the time intervals the electromagnetic signal requires to travel through the paths transceiver-intruder-transceiver and transceiver-intruder-receivers, forming, this way, a non-linear system of equations (involving circle and ellipses equations, respectively).

In order to estimate the intruder position, the PSO method is used and a new methodology was conceived. The main idea is to apply PSO to determine the equidistant point to the circle and to the two ellipses generated by using the data extracted from received transient signals (those three curves usually does not have a single interception point for highly

scattering environments). The equidistant point, determined via PSO, is the position estimative for single radar.
For a radar network, which is necessary for a large area under monitoring, the transmitters should operate in TDM (Time-Division Multiplexing) mode in order to avoid interference among them. For each possible transceiver-receivers combination, an estimate is obtained and, from the set of estimations, statistical parameters are calculated and used in order to produce a unique prediction of the intruder's position.

2. The FDTD Method and its Applications

The FDTD Method (Finite-Difference Time-Domain) had its first application in the solution of Maxwell's equations, in 1966, when Kane Yee used it in the analysis of spread of electromagnetic waves through bidimensional structures (Yee, 1966). This technique defines the spacial positioning of the components of the electric and magnetic fields in such a way that Ampère and Faraday laws are satisfied, and it approaches the derivates, constituents of those equations, by centered finite differences, in which the updating of the components of the electric fields is alternately verified in relation to those of the magnetic fields, by forming this way what is known as the algorithm of Yee. The method constitutes a solution of complete wave, in which the reflection, refraction, and diffraction phenomena are implicitly included.
Years passed by and, along with them, several scientific advances contributed to the establishment of this method as an important tool in the analysis and synthesis of problems in electromagnetism, among them it is noted: new high speed computers and auto-performance computer networks; the expansion of the method for the solution of problems in the 3D space, with the inclusion of complex materials, and the condition of stability (Taflove & Brodwin, 1975); development of truncation techniques of the region of analysis, known as ABC´s (Absorbing Boundary Conditions), such as the operators of Bayliss-Turkel Bayliss, & Turkel, (1980), Mur of first and second orders (Mur, 1981), Higdon technique (Ridon, 1987), Liao (Liao, 1987), PML of Berenger (Berenger, 1994), and the UPML of Sacks (Sacks et al., 1995).
The FDTD method, for its simplicity of application, strength and application in all spectrum of frequencies, has been used in the solution of antenna problems (Zhang et al., 1988), circuit analysis in high frequencies (Fornberg et al., 2000), radars (Muller et al., 2005), photonic (Goorjian & Taflove, 1992), communication systems (Kondylis et al., 1999), periodic structures (Maloney & Kesler, 1998), medicine (Manteuffell & Simon, 2005) , electric grounding system (Tanabe, 2001) , etc.

2.1 The Yee's Algorithm

Equations (1) and (2) represent the equations of Maxwell in its differential form, where **E** and **H** are the vectors intensity of electric and magnetic fields, respectively, μ is the magnetic permeability, ε is the electric permittivity of the medium and **J** is the current density vector. For the solution of these equations by the FDTD method, Kane Yee (Yee, 1966) proposed that the components of **E** (E_x, E_y, E_z) and **H** (H_x, H_y, H_z) were positioned in the space as it shown in Fig. 1.

$$\nabla x\mathbf{E} = -\mu\frac{\partial \mathbf{H}}{\partial t} \tag{1}$$

$$\nabla \mathrm{x}\mathbf{H} = \varepsilon \frac{\partial \mathbf{E}}{\partial \mathrm{t}} + \mathbf{J}. \tag{2}$$

Such procedure is justified by the necessity of agreement with the mathematical operators indicated in the equations above.

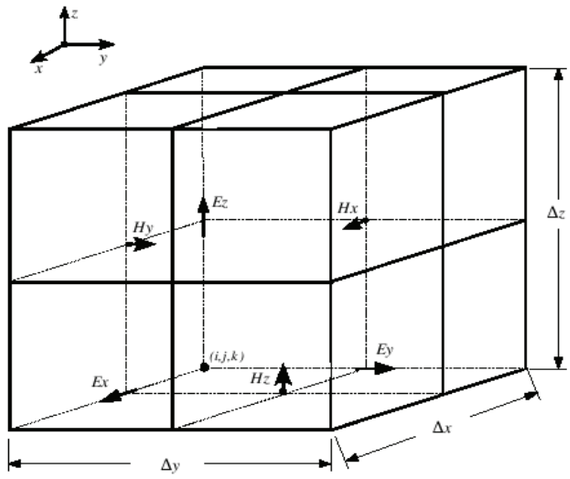

Figure 1. The Yee's Cell

This way, by expanding the curl operators in (1) and (2), it results in the following scalar equations

$$\frac{\partial H_x}{\partial t} = \frac{1}{\mu}\left(\frac{\partial E_Y}{\partial z} - \frac{\partial E_z}{\partial y}\right), \tag{3.a}$$

$$\frac{\partial H_y}{\partial t} = \frac{1}{\mu}\left(\frac{\partial E_z}{\partial x} - \frac{\partial E_x}{\partial z}\right), \tag{3.b}$$

$$\frac{\partial H_z}{\partial t} = \frac{1}{\mu}\left(\frac{\partial E_x}{\partial y} - \frac{\partial E_y}{\partial x}\right), \tag{3.c}$$

and

$$\frac{\partial E_x}{\partial t} = \frac{1}{\varepsilon}\left(\frac{\partial H_y}{\partial z} - \frac{\partial H_z}{\partial y} - \sigma E_x\right) \tag{4.a}$$

$$\frac{\partial E_y}{\partial t} = \frac{1}{\varepsilon}\left(\frac{\partial H_x}{\partial z} - \frac{\partial H_z}{\partial x} - \sigma E_y\right), \tag{4.b}$$

$$\frac{\partial E_z}{\partial t} = \frac{1}{\varepsilon}\left(\frac{\partial H_y}{\partial x} - \frac{\partial H_x}{\partial y} - \sigma E_z\right), \tag{4.c}$$

respectively.

The derivates in (3) and (4) are then approximated by central finite differences, in the following way

$$\frac{\partial F}{\partial l} \simeq \frac{F(l+\frac{1}{2}\Delta l) - F(l-\frac{1}{2}\Delta l)}{\Delta l} \tag{5}$$

where F represents any component of either electric or magnetic field and l can be x, y, z or t. By applying (5) in (3) and (4), it results in the updating equations of the components of fields given by (6)-(7), as follows.

$$H_x^{n+\frac{1}{2}}(i,j,k) = H_x^{n-\frac{1}{2}}(i,j,k) + \frac{\Delta_t}{\mu}\left[\frac{E_y^n(i,j,k+1) - E_y^n(i,j,k)}{\Delta_z} - \frac{E_z^n(i,j+1,k) - E_z^n(i,j,k)}{\Delta_y}\right], \tag{6.a}$$

$$H_y^{n+\frac{1}{2}}(i,j,k) = H_y^{n-\frac{1}{2}}(i,j,k) + \frac{\Delta_t}{\mu}\left[\frac{E_z^n(i+1,j,k) - E_z^n(i,j,k)}{\Delta_x} - \frac{E_x^n(i,j,k+1) - E_x^n(i,j,k)}{\Delta_z}\right], \tag{6.b}$$

$$H_z^{n+\frac{1}{2}}(i,j,k) = H_z^{n-\frac{1}{2}}(i,j,k) + \frac{\Delta_t}{\mu}\left[\frac{E_x^n(i,j+1,k) - E_x^n(i,j,k)}{\Delta_y} - \frac{E_y^n(i+1,j,k) - E_y^n(i,j,k)}{\Delta_x}\right], \tag{6.c}$$

and

$$E_x^{n+1}(i,j,k) = E_x^n(i,j,k)\left(\frac{1-\sigma\frac{\Delta_t}{2\varepsilon}}{1+\sigma\frac{\Delta_t}{2\varepsilon}}\right) + \frac{\Delta_t}{\varepsilon\left(1+\sigma\frac{\Delta_t}{2\varepsilon}\right)}\left[\frac{H_z^{n+1/2}(i,j,k) - H_z^{n+1/2}(i,j-1,k)}{\Delta_y} - \frac{H_y^{n+1/2}(i,j,k) - H_y^{n+1/2}(i,j,k-1)}{\Delta_z}\right], \tag{7.a}$$

$$E_y^{n+1}(i,j,k) = E_y^n(i,j,k)\left(\frac{1-\sigma\frac{\Delta_t}{2\varepsilon}}{1+\sigma\frac{\Delta_t}{2\varepsilon}}\right) + \frac{\Delta_t}{\varepsilon\left(1+\sigma\frac{\Delta_t}{2\varepsilon}\right)}\left[\frac{H_x^{n+1/2}(i,j,k) - H_x^{n+1/2}(i,j,k-1)}{\Delta_z} - \frac{H_y^{n+1/2}(i,j,k) - H_y^{n+1/2}(i-1,j,k)}{\Delta_x}\right], \tag{7.b}$$

$$E_z^{n+1}(i,j,k) = E_z^n(i,j,k)\left(\frac{1-\sigma\frac{\Delta_t}{2\varepsilon}}{1+\sigma\frac{\Delta_t}{2\varepsilon}}\right) +$$

$$+\frac{\Delta_t}{\varepsilon\left(1+\sigma\frac{\Delta_t}{2\varepsilon}\right)}\left[\frac{H_y^{n+1/2}(i,j,k)-H_y^{n+1/2}(i-1,j,k)}{\Delta_x}\right. \quad (7.c)$$

$$\left.-\frac{H_x^{n+1/2}(i,j,k)-H_x^{n+1/2}(i,j-1,k)}{\Delta_y}\right],$$

where i,j,k and n are integers; i,j,k are indexes for the spatial coordinates x, y and z and n is the temporal index for the time t, in such way that $x = i\Delta_x$, $y = j\Delta_y$, $z = k\Delta_z$ and $t = n\Delta_t$ (Δ_x, Δ_y and Δ_z are the spatial increments and Δ_t is the time step).

2.2 Precision and Stability

The precision represents how close the obtained result is to the exact result, and the stability is the guarantee that the solution of the problem will not diverge. In order to precision and stability to be guaranteed, the following criteria are adopted in this work (Taflove & Hagness 2005):

$$\Delta_{x,y,z} \leq \frac{\lambda_{min}}{10}$$

and

$$\Delta_t \leq \frac{1}{v_{max}\sqrt{\frac{1}{(\Delta_x)^2}+\frac{1}{(\Delta_y)^2}+\frac{1}{(\Delta_z)^2}}}.$$

which means that the minimum wave length existing in the work environment has to be characterized by, at least, 10 cells (Taflove & Hagness 2005). Depending on the application, this number can be superior to 100, and the time increment will be limited by the maximum distance to be travelled, by the respective wave, in the cell of Yee (Taflove & Hagness 2005).

2.3 The Sacks' Uniaxial Perfecttly Matched Layers

One of the problems of the numeric methods is the fact that they do not offer resources that permits the interruption of the spacial iterative process. This causes the method to be limited, mainly when the solution of open problems is taken into account. In order to solve this problem, several techniques have been developed, among them there is the UPML (Uniaxial perfecttly matched layers) (Sacks et al., 1995), which was used in this work. This method takes into account, around the region of analysis (Fig.2), layers perfectly matched, constituted by anisotropic media and with loss, which are characterized by the following equations of Maxwell, in the frequency domain.

$$\nabla x\mathbf{E} = -j\omega\mu[s]\mathbf{H} \quad (8)$$

$$\nabla x\mathbf{H} = j\omega\varepsilon[s]\mathbf{E}, \quad (9)$$

where the tensor $[s]=\begin{bmatrix} \frac{s_y s_z}{s_x} & 0 & 0 \\ 0 & \frac{s_x s_z}{s_y} & 0 \\ 0 & 0 & \frac{s_x s_y}{s_z} \end{bmatrix}$, with $s_\alpha = 1 + \frac{\sigma_\alpha}{j\omega\varepsilon_0}$, in which σ_α is the attenuation electric conductivity in the directions α = x, y, z, introducing the anisotropy in the medium. **E** and **H** are the vectors intensity of electric and magnetic field in the frequency domain, respectively.

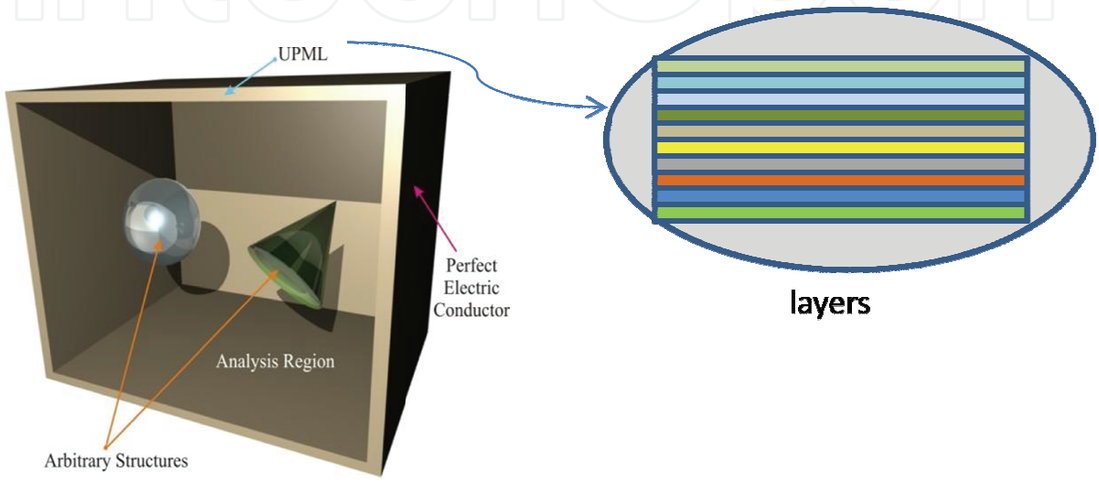

Figure 2. The analysis region limited by UPML

In order to avoid the use of convolution in the transformation of the equations above into the time domain, one defines the following constitutive relations:

$$D_x = \varepsilon\left(\frac{s_y}{s_x}E_x\right), D_y = \varepsilon\left(\frac{s_z}{s_y}E_y\right), D_z = \varepsilon\left(\frac{s_x}{s_z}E_z\right); \quad (10)$$

$$B_x = \mu\left(\frac{s_y}{s_x}H_x\right), B_y = \mu\left(\frac{s_z}{s_y}H_y\right), B_z = \mu\left(\frac{s_x}{s_z}H_z\right), \quad (11)$$

where D_x, D_y, D_z and B_x, B_y, B_z are the components of the vectors electric flux density (**D**) and magnetic (**B**), respectively. In order to find the updating equations for the components of the electric field, the updating equations for D_x, D_y and D_z, have to be found first, which is done by the substitution of [s] in (9), considering (10). Next, the components of **E** are found through eq. (10). The same procedure is done in order to find the components of **H** (Taflove & Hagness, 2005).

3. Particle Swarm Optimization and Radar Applications

3.1 Basic Radar Theory Overview

The main reason for using radars is to determine the spatial position of an object. This is performed by transmitting electromagnetic pulses through space, which will be scattered by

the target and by other objects. Transient responses obtained at certain points in space are used to determine the target's position.

In particular, multistatic radars can be composed by a transceiver (transmitter and receiver at the same point – Tx/Rx1) and, at least, two remote receivers (Rx2 and Rx3), such as illustrated by Fig. 4. The signal leaves the transceiver and reaches the target, which reflects it toward the receivers and the transceiver as well.

From the transceiver perspective, the signal takes a certain amount of time for returning. This only means that the target could be at any point of a circle centered at the transceiver's coordinates (Fig. 4). Longer the time, larger is the circumference. From the receiver perspective, the signal travels from the transmitter, it reaches the target and then it arrives at the receiver coordinates. This only means that the target is at the locus defined by an ellipse with foci at the transceiver's and at the receiver's coordinates (Fig. 3). Of course, longer the propagation time, greater is the total path (calculated by using time and the propagating speed) and larger is the ellipse's semiminor axis. The solution of the system of equations this way composed provides the target's position.

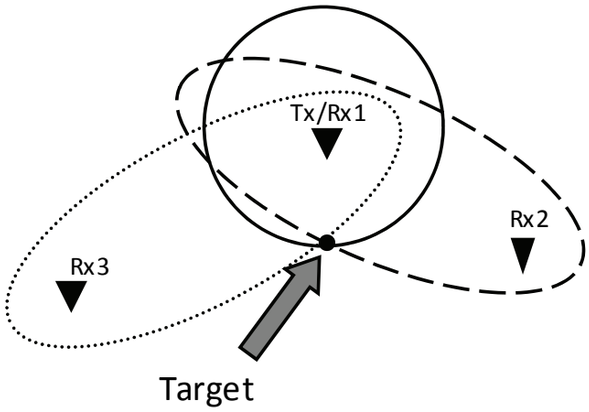

Figure 3. Ideal multistatic radar

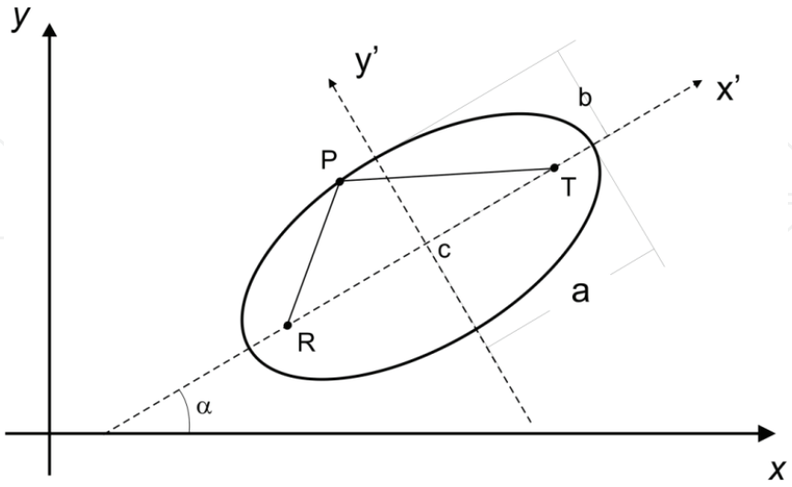

Figure 4. The ellipse's parameters

Fig. 4 shows the ellipse's basic parameters (T indicates the transceiver position, R indicates the receiver's, position and P defines the intruder's location).

The ellipse equation is given by

$$\boldsymbol{F_n(x,y) = A_n^2(x,y) + B_n^2(x,y) - C_n^2 = 0}, \tag{12}$$

where

$$\boldsymbol{A_n(x,y) = a_n\left[(y - y_{c_n})\cos\alpha_n - (x - x_{c_n})\sin\alpha_n\right]}, \tag{13}$$

$$\boldsymbol{B_n(x,y) = b_n\left[(x - x_{c_n})\cos\alpha_n - (y - y_{c_n})\sin\alpha_n\right]} \tag{14}$$

and

$$\boldsymbol{C_n = a_n b_n}, \tag{15}$$

in which a is the semimajor axis, b is the semiminor axis, x_c and y_c are the coordinates of the center C of the ellipse, and α is the angle from the x-axis to the ellipse's semimajor axis. Here, n is the receiver identifier (index). The parameters x_{Cn}, y_{Cn}, a_n, b_n and α_n are calculated by

$$\boldsymbol{x_{c_n} = \frac{1}{2}(x_T + x_{R_n})}, \tag{16}$$

$$\boldsymbol{y_{c_n} = \frac{1}{2}(y_T + y_{R_n})}, \tag{17}$$

$$\boldsymbol{a_n = \frac{1}{2}(d_{TPR_n})}, \tag{18}$$

$$\boldsymbol{b_n = \frac{1}{2}\left(\sqrt{d_{TPR_n}^2 - d_{TR_n}^2}\right)}, \tag{19}$$

$$\boldsymbol{d_{TR_n} = \sqrt{(x_T - x_{R_n})^2 + (y_T - y_{R_n})^2}}, \tag{20}$$

$$\boldsymbol{\alpha_n = \tan^{-1}\left(\frac{y_T - y_{R_n}}{x_T - x_{R_n}}\right)}. \tag{21}$$

were x_T and y_T are the coordinates of the transmitter, x_R and y_R are the coordinates of the receiver R and d_{TR} is the distance from the receiver to the transmitter. Finally, d_{TPR} is given

by the sum of the lengths of the segments $\overline{TP}$ and $\overline{TR}$ (the total path length), estimated from the propagation time.
The calculation of the propagation time is performed by two steps: 1) by sending a pulse and registering the transient response at the transceiver and at the receivers and 2) by sending a second pulse and subtracting the new obtained registers from the previously recorded set. Of course, it is assumed that the target is in movement; otherwise the data obtained from steps 1) and 2) would be identical. If the pulse is UWB, it is possible to detect the movement of the heart of a human intruder, meaning he would be a detectable target even if he kept perfectly static.

3.2 Particle Swarm Optimization

The particle swarm optimization (PSO) method is a modern heuristic optimization algorithm, based on group movement of animals, such as fishes, birds and insects. The movement of each animal (individual or particle) can be seen as a resultant vector of personal and collective characteristics (vector components).
Proposed in (Kennedy & Eberhart, 1995), this method consists on the optimization of an objective function trough the exchange of information among the particles (individuals), resulting in a non-deterministic, but robust and efficient algorithm, which can be easily implemented computationally.
In an initial moment, all the particles are positioned randomly in the searching space, in which the solution must be. The movement of each particle is the result of a vector sum of three distinct terms: the first contribution is related to the inertia of the particle (a particle's personal component), the second is related to the best position occupied by the particle (a personal component - memory) and the third is relative to the best position found by the group (group contribution – cooperation). Each particle position (a multidimensional vector) corresponds to an alternative solution for the problem (combination of the multidimensional vector). Each alternative solution must be evaluated.

Thus, at a given time step, a particle *i* changes its position from $\vec{X}_i$ to $\vec{X}_i^{new}$ according to

$$\vec{X}_i^{new} = \vec{X}_i + \vec{\Delta}_{x,i}, \tag{22}$$

in which $\vec{\Delta}_{x,i}$ is the updated position increment for particle *i*, that is, it is the vector representing the position change for particle *i* and it is given by

$$\vec{\Delta}_{x,i} = \vec{\Delta}_{x,i}^{old} + U.W_{m,i}(\vec{b}_i - X_i) + U.W_{c,i}(\vec{b}_g - X_i) \tag{23}$$

The heights $W_{m,i}$ (memory) and $W_{c,i}$ (cooperation) are previously defined, U represents independent samples of a random variable uniformly distributed between zero and one, $\vec{b}_i$ is the best solution found by the particle *i* and $\vec{b}_g$ is the best solution found by the swarm, up to the current interaction.

The initial values for the displacements, i.e. $\vec{\Delta}_{x,i}^{old}$, are randomly chosen among the real values limited by $-\vec{\Delta}_x^{\max}$ and $\vec{\Delta}_x^{\max}$, in order to avoid large values and the consequent divergence from the solution. It is worth to mention that it is necessary to avoid such large values during the interactions. It was observed that usually the method results in divergence or in low precision due to this tendency. There are, however, some methods for minimize these problems, such as:

1. The employment of a descending function, affecting the inertial term, such as an evanescent exponential function of time;
2. The use of terms for reduction of the velocity at each interaction, known as constriction terms.
3. Simply to limit each velocity component to the interval $[-\vec{\Delta}_x^{\max}, \vec{\Delta}_x^{\max}]$.

All the methods have been tested, and, although all of them were efficient, the last one was applied here.

3.3 Estimation of the Intruder's Position with PSO

After obtaining the time responses with the FDTD method, the radar theory can be employed. The parameters of the three curves (a circle and two ellipses) are calculated from the differences of the time responses (with and without the intruder), and the obtained system, when solved, deliveries the intruder's position estimation. However, the case where the three curves have a common point (Fig. 5a) does not always happen and the more frequent case is illustrated by Fig. 5b. This way, the objective of the PSO algorithm is to locate the point with the minimal distance from the three curves simultaneously. This defines the objective function, which is mathematically given by

$$F_i = d_i C_{min} + d_i E^1_{min} + d_i E^2_{min}, \tag{24}$$

in which $d_i C_{min}$ is the minimal distance from particle i to the circle and $d_i E^{\kappa}_{min}$ is the minimal distance from particle i to the ellipse κ.

This way, the PSO algorithm acts towards the minimization of the objective function F_i.

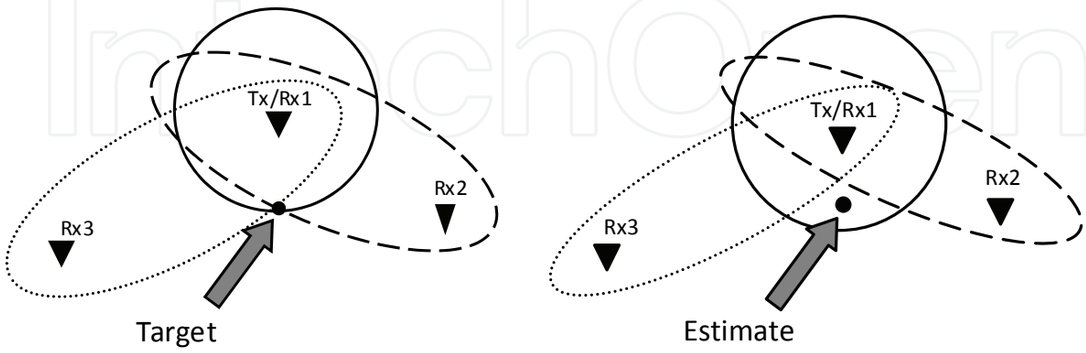

(a) (b)

Figure 5. Ideal radar configuration and (b) real radar configuration and the position estimate (objective of the PSO Locator)

In order to create a more realistic situation, additive Gaussian white noise (AWGN) has been added to the FDTD time responses. A sample of noise $\mathbf{R}(\xi)$ is generated by

$$\mathbf{R}(\xi) = \sigma_a \sqrt{2\ln\left[1/(1-\mathbf{U}(\xi_j))\right]}\cos\left[2\pi\mathbf{U}(\xi_k)\right], \tag{25}$$

in which σ_a = 0.02 for the present work, and U(ξ) has the same meaning of *U* in (23).

3.4 Estimation of the numerical velocity for distance calculations.

FDTD Method introduces numerical dispersion and numerical anisotropy for the propagating waves. This means that velocity of propagation is a function of frequency and of the propagation direction (Taflove & Brodwin, 1975.a). Due to this numerical characteristic of the FDTD methodology, it is not appropriate to use the light free space velocity. Besides that, the dielectric walls promote delays on the signals, affecting the average velocity. This way, as detailed in (Muller et al., 2005), and effective velocity was determined experimentally for calculating the ellipses parameters (distances). The idea is to measure the propagating time in multiple points around the source, with and without walls, and take an average of the obtained velocities (Muller et al., 2005).

It is worth to mention that the procedure presented in (Muller et al., 2005) takes automatically into account numerical dispersion and anisotropy and the delays caused by walls. In real applications, obviously only walls' delays must be considered for the correct operation of the radar system.

4. Environment and Parameters of Simulation

In this work, the indoor environment considered for the simulations is shown in Fig. 6. In that building, there are two distinct kinds of walls, characterized by different electrical parameters, which are: the relative electric permittivity of the exterior walls is ε_r= 5.0 and those of the interior walls have ε_r= 4.2. In both of them, the chosen conductivity is σ= 0.02 S/m. Everywhere else, the relative permittivity is equal to unity, except in the UPML. The thickness of walls are 27 (external) and 12 (internal) centimeters.

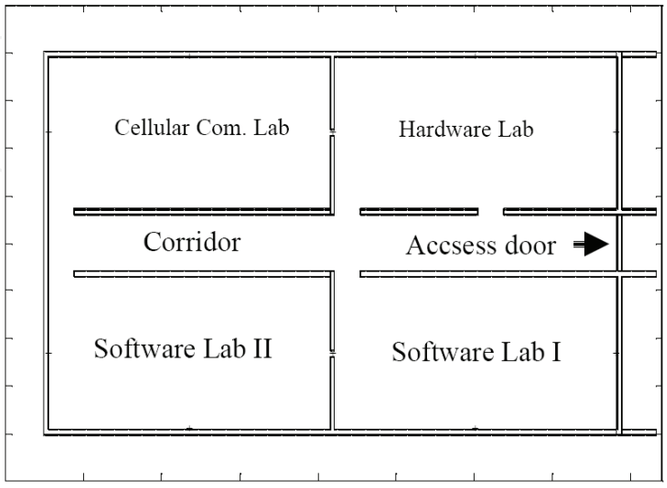

Figure 6. Layout of the building (floor plan)

The simulations are performed using a 2D-FDTD method for nondispersive isotropic media (analysis region), based on Yee's formulation. It is worse to mention that only perpendicular polarization relative to the plan in Fig. 6 is considered in the transmitter antenna. Here, an uniform mesh with 1000×1000 cells was used. The square-shaped cells have 1.5 cm $(\Delta_x = \Delta_y = \Delta_s)$ of width, which is equivalent to approximately one-tenth of the free-space wavelength of the excitation pulse in the reference frequency f_o = 2 GHz. The time increment was obtained from the spacial cell dimension , in order to assure the numerical stability of the method. The value used in this paper is given by

$$\Delta t = 0.7 \frac{\Delta s}{c\sqrt{2}} \tag{26}$$

where c is the speed of light in vacuum. Equation (26) is the Courant's condition (Taflove & Brodwin, 1975.a).

The absorbing boundaries are very important elements in the FDTD mesh (see section 2). Their purpose is to limit the computational domain and, thus, to simulate propagation in an open environment, with minimum reflection. In order to achieve this, an anisotropic perfectly matched layer-absorbing medium (UPML) based on a lossy uniaxial medium is used. The parameters of the UPML are: Thickness d = 10 cells, maximum attenuation conductivity σ_{max} = 15 S/m, and order of polynomial variation m=4.

The waveform used as an excitation source, in order to scan the environment, is the Gaussian monocycle, shown in Fig. 7.

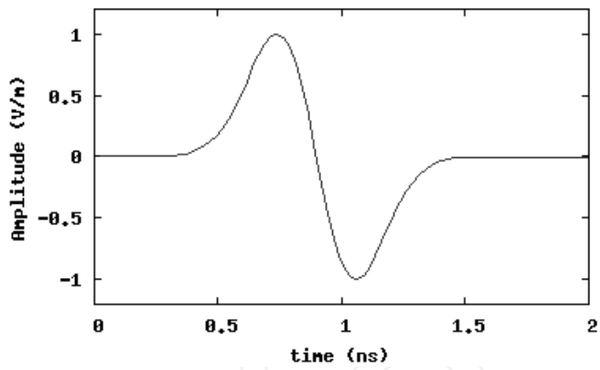

Figure 7. Gaussian monocycle pulse

This is the type of pulse is used, for example, in PulsON system (Petroff & Withington, 2001). It is obtained from the following Gaussian function:

$$g(t) = A_0 Exp\left[\frac{-(t-t_0)^2}{\tau^2}\right] \tag{27}$$

where A_0 is the maximum amplitude of the excitation source, t_0 is the time when the maximum amplitude occurs, and τ is the time-decay constant. The Gaussian monocycle is the first derivative of this function, that is:

$$p(t) = -A_p \sqrt{\frac{2e}{\tau^2}}(t-t_0) exp\left[-\frac{(t-t_0)^2}{\tau^2}\right], \tag{28}$$

Where $e \approx 2.71828$ and A_p is the peak amplitude of the monocycle. A_p and A_0 are related by

$$A_0 = A_p \tau \sqrt{\frac{e}{2}} \tag{29}$$

The Gaussian monocycle is an ultra-wideband signal, with the bandwidth and central frequency dependent on the duration of the monocycle. In the frequency domain, the spectrum obtained from its Fourier transform is given by

$$p(f) = A_p \tau^2 \sqrt{\frac{\pi e}{2}} exp\left[1-(\pi\tau f)^2\right] exp(-j2\pi t_0 f) \tag{30}$$

and the central frequency of the monocycle can be calculated using the following equation:

$$f_0 = \frac{1}{\tau\sqrt{2\pi^2}} \ . \tag{31}$$

The monocycle spectrum is shown by Fig. 8. Observe the significant power is distributed up to the frequency 2 GHz, which is the frequency used for determining Yee's spatial increment Δs .

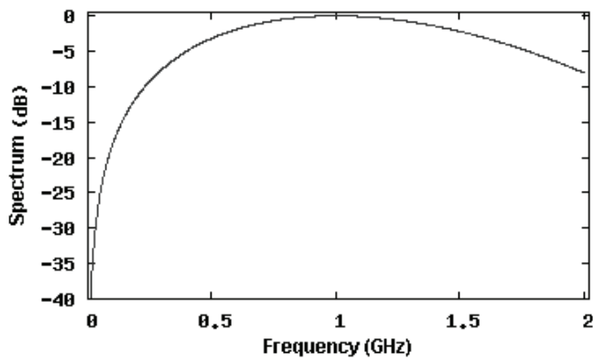

Figure 8. The Gaussian monocycle spectrum

To complete the environment description, the only missing item is the target. It was chosen to be a cylinder with a 0.25 m radius (in fact, only its transversal section is considered, since the mesh has two dimensions), with the aim of representing a human body. The relative permittivity considered is $\varepsilon_r = 50$ and the conductivity $\sigma = 1.43 \ \ S/m$ (Gandhi & Lazzi, 1996).

5. Results

For our numerical simulations, we chose different positions of the target in order to investigate some critical situations in the sense of errors of the position estimation. For computer implementation, we need to choose also some parameters, which have not been specified yet. For PSO, we define the following weights for particles: $W_m = W_c = 10^{-2}$ and the maximum value for the parameter $\vec{\Delta}_{x,i}$ is 10^{-2}. These parameters have been defined empirically. The total number of particles is 100 and the maximum number of PSO iterations

is 2000. An unfavorable situation of the target position is shown in Fig. 9. The transceivers are denoted by TRX1 and TRX2. The remote receivers are denoted by RX2,..., RX9. When a transceiver is transmitting, its receiver is denoted by RX1. The transceivers are activated in different time windows in accordance with TDM (time division multiplexing) scheme. The target, in this case, is on the line connecting the two transceivers, and it is situated outside the rooms where the transceivers are mounted.

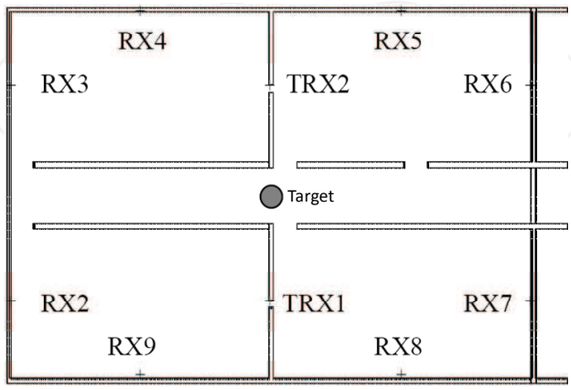

Figure 9. An unfavorable position for the target and the radar elements' positions

The transmitting antennas are initially positioned in small windows in the walls (Fig. 9). Because of the diffraction in these windows, we can expect a larger estimation error as compared to the more favorable configurations. Fig. 10 shows the set ellipses for this case. There is a considerable dispersion of the ellipses. The estimated error for this situation is about 17 cm, but even in this case one can still consider the precision of the target position estimation as rather good. Of course, more favorable conditions generate results with better precision.

In this work, the final estimation of the position is obtained from statistically treating the responses obtained from all the possible combinations of multistatic radars (one transceiver and two receivers). The mean and standard deviation of the estimates are calculated. All the estimative outside the standard deviation, around the mean value, are not considered in the calculation of the final mean, which is the final output of the estimator.

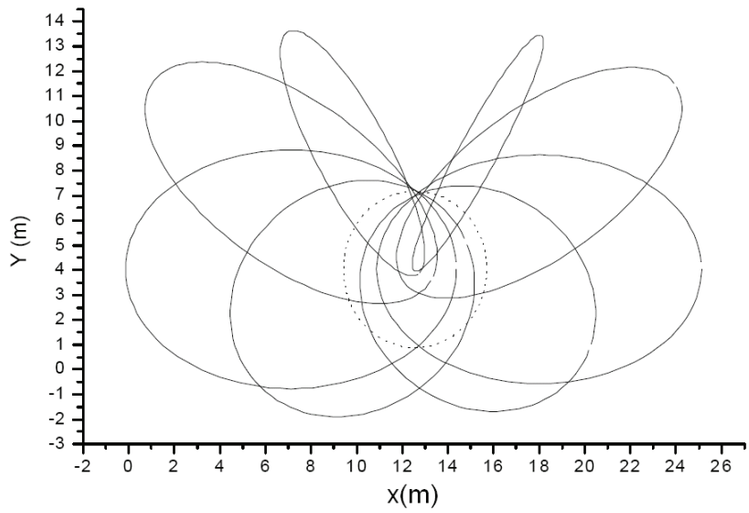

Figure 10. The set of ellipses obtained for locating the target

Fig. 11 shows the convergence of the PSO method for a single multistatic radar (the transceiver and two receivers). It is evident that the algorithm can be employed for solving this kind of problem, as far as the particles clearly move to the correct target's position. Similar behavior was observed in many other experiments.
Fig. 12 shows the transient electric field obtained by receiver 4 (see Fig. 9), in the presence of the target and in its absence. It is clear the perturbation caused in the reference signal by the dielectric cylinder. The perturbation (difference between the signals) is plotted in Fig. 13, from which the temporal information necessary for defining the ellipse with focus in that receiver and in the transceiver (when disturbance's amplitude is different from zero).

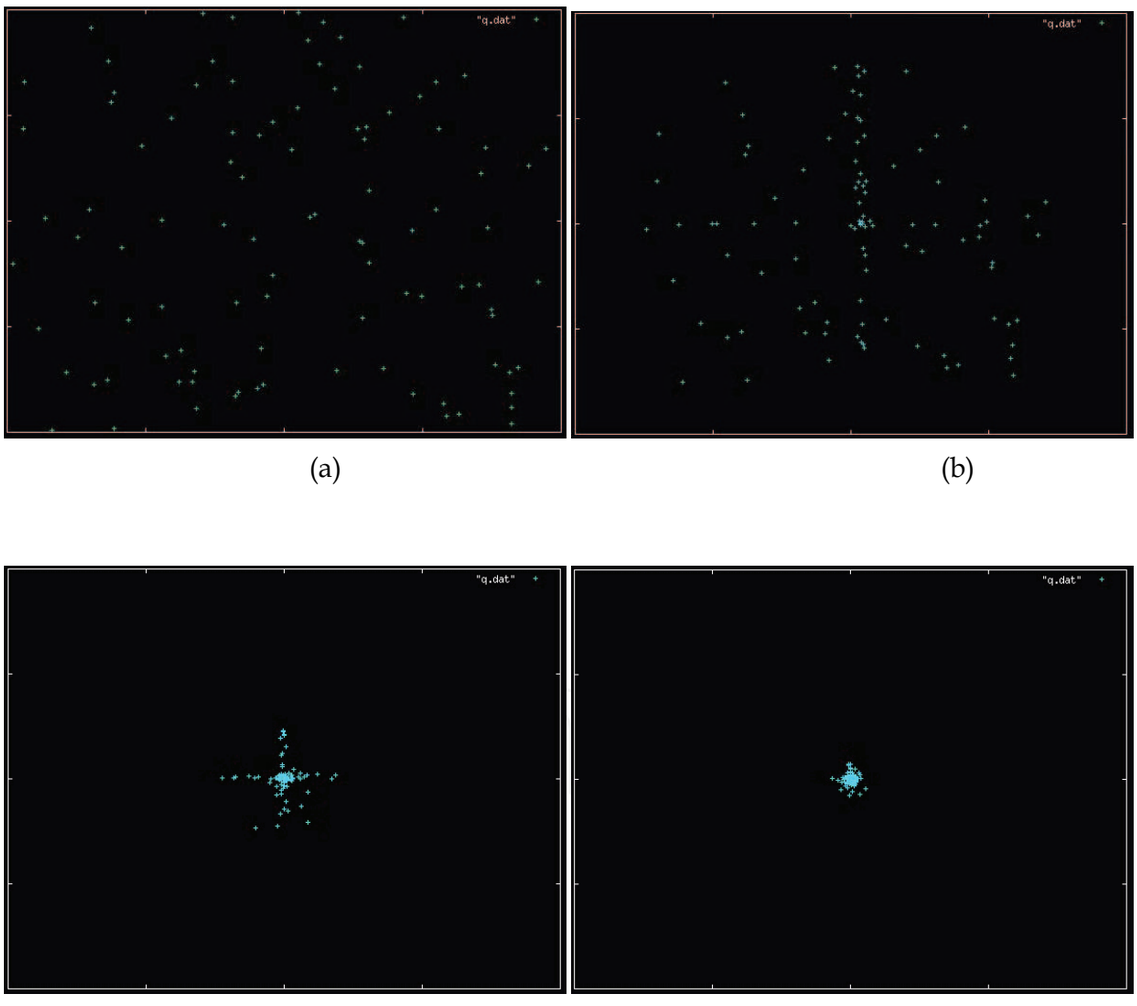

Figure 11. PSO's particles convergence for the location of the target (a) randomly distributed particles; (b) particles' positions after 100 interactions; (c) particles' positions after 500 interactions and (d) particles' positions after 700 interactions

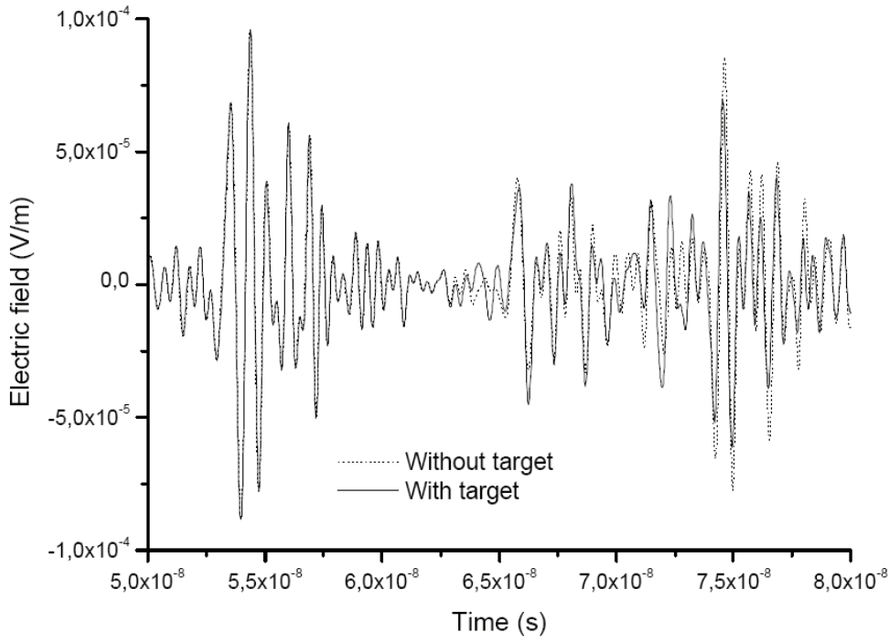

Figure 12. Electric field data obtained by the receiver 4 (with and with no target)

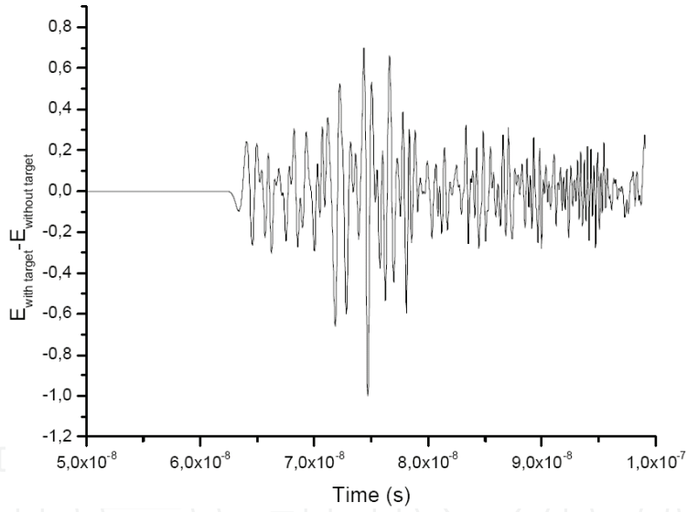

Figure 13. Difference between the signals depicted in Fig. 12 (disturbance caused by the target)

Fig. 14(a) shows the configuration used for executing a second numerical experiment. In this case, the transceivers TRX1 and TRX2, represented by rhombuses, are positioned away from the walls. The receivers (represented by triangles) and the target (square) were positioned exactly as in the previous case (Fig. 9). For the case illustrated by Fig. 15(a), in which it is used only the transceiver TRX1, the PSO estimation is represented by the star (the estimated position was (432.98,410.92)) . The central cell of the target is (460,450) and, this way, the surface of the target was pointed out, as it is clearly shown by Fig. 15(a). Similar behavior was observed for the case illustrated by Fig. 15(b), in which only the transceiver TRX2 is used. It is worth to mention that the identified points of the target's surface is, for each

simulation, closer to the correspondent used transceiver. This behavior is expected, as long as reflection is used for determining the propagation time used for calculating the circle's and the ellipses' parameters.

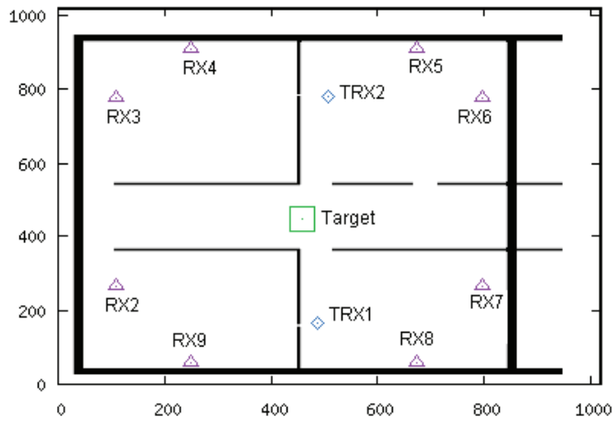

Figure 14. Configuration used for the second experiment (axis represent the Yee's cells indexes)

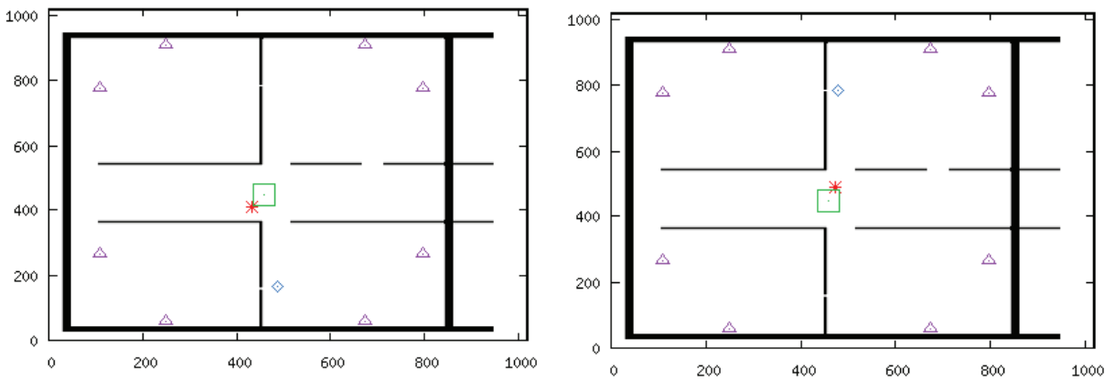

(a) (b)

Figure 15. The PSO estimation for the second experiment (a) result obtained by using TRX1 and (b) result obtained by using TRX2

In order to increase the complexity of the environment, and for testing a more general situation, scatters were introduced in the environment and the situation previously analyzed was used as base for the configuration shown by Fig. 16, which defines the third experiment. Each scatter consists of a dielectric material with electrical conductivity of 0.02 S/m and permittivity of $5.\varepsilon_0$. The diameters of the dielectric scatters are around 18 centimeters. Such scatters create a chaotic electromagnetic environment, generating multiple reflections, refractions and delays on the propagation of the wave. As far as difference of electromagnetic transients are considered for calculating the propagation periods, such effects are suppressed and the obtained results are very similar to the previous experiment responses, as shown by Figs. 16(a) and 16(b).

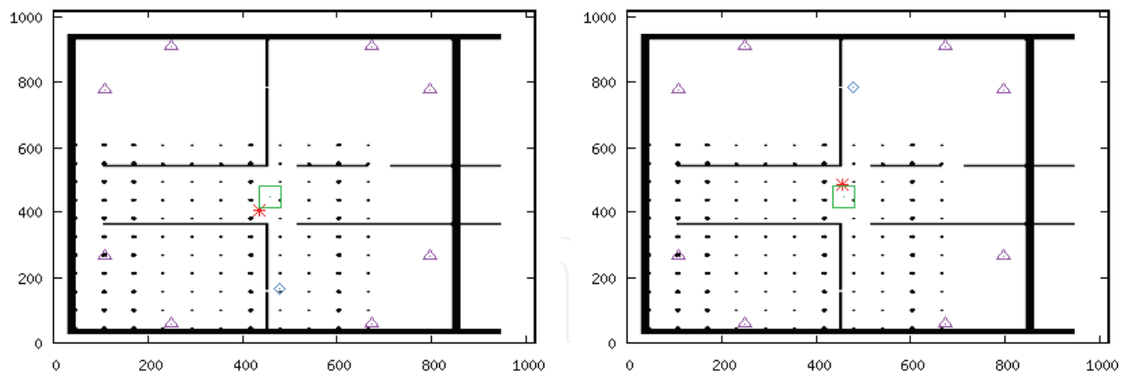

(a) (b)

Figure 16. The PSO estimation for the third experiment (with dielectric scatters) (a) result obtained by using TRX1 and (b) result obtained by using TRX2

6. Final Remarks

We have presented in this work some results of numerical simulations of a radar array based on UWB pulses. The registers of the electric field have been obtained numerically using the FDTD method. In order to define the localization curves we have used the concept of optic rays. The solutions of the system of the nonlinear equations (which usually does not exist) defined for every combination of a transceiver and 2 remote receivers give an estimation of the target position. The solution, in those cases, are defined by determining the closest point in the space to the circle and for the two ellipses, for a single multistatic radar. The final estimation for the array of two transceivers and eight receivers is fulfilled by PSO method. We have shown that PSO is a useful tool for this type of problem. The proposed methodology seems to be robust, as long as the presence of dielectric scatters, which promotes a complex (chaotic) electromagnetic environment, does not substantially affects the performance of the position estimator.

7. Acknowledgements

Authors would like to acknowledge the support provided by Federal University of Pará (UFPA), for all infrastructure provided.

8. References

Bayliss, A. & Turkel, E. (1980). Radiation Boundary Conditions for wave-like equation, *Comm. Pure Appl. Math.*, vol. 23, pp. 707-725

Berenger, J. (1994). A perfectly matched layer for the absorption of electromagnetic waves, *J. Computational Physics*, vol. 114, pp. 185-200

Fornberg, P.E.; Byers, A.; Piket-May, M. & Holloway, C.L.(2000). FDTD modeling of printed circuit board signal integrity and radiation, *IEEE International Symposium on Electromagnetic Compatibility*

Gandhi, O. P.; Lazzi G. & Furse, C. M (1996). *Electromagnetic absorption in the human head and neck for mobile telephones at 835 and 1900 MHz,* IEEE Trans. Microwave Theory and Tech., vol. MTT-44, No. 10.

Goorjian, P.M. & Taflove, A. (1992). Direct time integration of Maxwell's equation in nonlinear dispersive media for propagation and scattering of femtosecond electromagnetic solitons, *Optics Lett*., vol. 17, pp. 180-182.

Liao , Z.; Wong, H.; Yang, B.P. & Yuan, Y.F. (1984). A Transmitting boundary for transient wave analysis, *Scientia Sinica*, vol. XXVII (series A), pp. 1063-1076

Maloney, J.G. & Kesler, M.P. (1998). Analysis of periodic structures. *Advances in Computational Electrodynamics*, A. Taflove, Artech House, 1998.

Manteuffell, D. & Simon W., FDTD calculation of the SAR induced in the human head by mobile phones: new standards and procedures for the numerical assessment, *IWAT 2005 (IEEE International Workshop on Antenna Technology)*, pp. 137-140.

Muller, F.C.B.F.; Farias, R.G.; Sobrinho, C.L.S.S. & Dmitriev, V. (2005). Multistatic radar with ultra wideband pulses: FDTD simulation, *International Microwave and Optoelectronic Conference*, Brasilia (Brazil)

Mur, G. (1981). Absorbing boundary conditions for the finite-difference approximation of the time-domain electromagnetic field equation, *IEEE Trans. Electromagnetic Compatibility*, vol. 23, pp. 377-382

Petroff,A. & Withington, P. (2001). PulsOn technology overview, 2001, *http://w.w.w.timedomain.com/ files/downloads/techpapers/PulsONOverview7_01.pdf*.

Ridon, R. (1987). Numerical absorbing boundary conditions for the wave equations, *Mathematics of computation*, vol. 49, pp. 65-90

Sacks, Z.; Kingsland, D.; Lee R. & Lee, J. (1995). A perfectly matched anisotropic absorber for use as an absorbing boundary condition, *IEEE Trans. Antennas and Propagation*, vol. 43, pp. 1460-1463

Taflove A. & Brodwin, M.E. (1975.a). Computation of the electromagnetic fields and induced temperatures within a model of the microwave-irradiated human eye, *IEEE Transaction on Microwave Theory Tech.*, vol. 23, pp. 888-896

Taflove, A & Hagness, S.C. (2005). *Computational Electromagnetics, The Finite-Difference Time-Domain Method*, 3rd ed., Artech House Inc..

Taflove A. & Brodwin, M.E. (1975.b). Numerical solution of steady-state electromagnetic scattering problems using the time-dependent Maxwell's equations, *IEEE Transaction on Microwave Theory Tech*., vol. 23, pp. 623-630

Tanabe, K.(2001). Novel method for analyzing the transient behavior of grounding systems based on the finite-difference time-domain method, *Power Engineering Review,* vol. 21, no. 9, pp. 1128-1132

Kennedy, J. & Eberhart, R. C., Particle swarm optimization, *IEEE International Conference on Neural Networks (ICNN),* Vol. IV, pp.1942-1948, Perth, Australia.

Kondylis, G.; DeFlaviis F. & Pottie, G. (1999). Indoor channel characterization for wireless communications using reduced finite difference time domain (R-FDTD), *IEEE VTC Fall 99,* Amsterdam.

Yee, k. (1996). Numerical solution of initial boundary value problems involving Maxwell's equations in isotropic media, *IEEE Trans. Antennas and Propagation,* vol. 14, pp. 302-307

Zhang X.; Fang, J.; Mei, K.K. & Liu, Y. (1988). Calculation of dispersive characteristics of microstrips by the Time-Domain Finite-Difference method, *IEEE Transaction on Microwave Theory Tech.*, vol. 36, pp. 263-267

Federal University of Pará
Electrical Engineering, CEP: 68455-700, Tucuruí, Pará, Brazil
Computer Engineering, CEP: 66075-900, Belém, Pará, Brazil
rmso@ufpa.br, leonidas@ufpa.br, josivaldo@lane.ufpa.br, rgfarias@ufpa.br

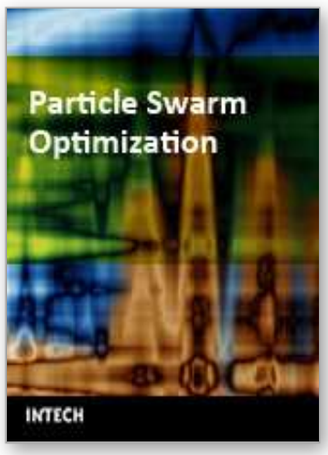

Particle Swarm Optimization

Edited by Aleksandar Lazinica

ISBN 978-953-7619-48-0
Hard cover, 476 pages
Publisher InTech
Published online 01, January, 2009
Published in print edition January, 2009

Particle swarm optimization (PSO) is a population based stochastic optimization technique influenced by the social behavior of bird flocking or fish schooling.PSO shares many similarities with evolutionary computation techniques such as Genetic Algorithms (GA). The system is initialized with a population of random solutions and searches for optima by updating generations. However, unlike GA, PSO has no evolution operators such as crossover and mutation. In PSO, the potential solutions, called particles, fly through the problem space by following the current optimum particles. This book represents the contributions of the top researchers in this field and will serve as a valuable tool for professionals in this interdisciplinary field.

InTech Europe
University Campus STeP Ri
Slavka Krautzeka 83/A
51000 Rijeka, Croatia
Phone: +385 (51) 770 447
Fax: +385 (51) 686 166
www.intechopen.com

InTech China
Unit 405, Office Block, Hotel Equatorial Shanghai
No.65, Yan An Road (West), Shanghai, 200040, China
中国上海市延安西路65号上海国际贵都大饭店办公楼405单元
Phone: +86-21-62489820
Fax: +86-21-62489821

IntechOpen